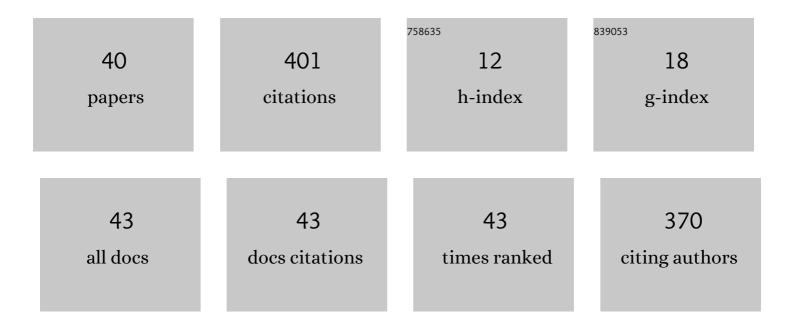
Bo Chen

List of Publications by Year in descending order

Source: https://exaly.com/author-pdf/7751723/publications.pdf Version: 2024-02-01



RO CHEN

#	Article	IF	CITATIONS
1	Solar X-ray and Extreme Ultraviolet Imager (X-EUVI) loaded onto China's Fengyun-3E Satellite. Light: Science and Applications, 2022, 11, 29.	7.7	7
2	The elastoplastic numerical model and verification by macroindentation experiment of femoral head. Computer Methods in Biomechanics and Biomedical Engineering, 2021, 24, 1-7.	0.9	0
3	SSDANet: Spectral-Spatial Three-Dimensional Convolutional Neural Network for Hyperspectral Image Classification. IEEE Access, 2020, 8, 127167-127180.	2.6	14
4	Photon Counting Imaging with Low Noise and a Wide Dynamic Range for Aurora Observations. Sensors, 2020, 20, 5958.	2.1	3
5	A method to derive global O/N2 ratios from SSUSI/DMSP based on Re-AURIC algorithm. Journal of Atmospheric and Solar-Terrestrial Physics, 2020, 199, 105196.	0.6	4
6	A High-Precision Flat Field Method Based on Image Stitching for Short Wavelength Instruments. Solar Physics, 2020, 295, 1.	1.0	3
7	Wide-field auroral imager onboard the Fengyun satellite. Light: Science and Applications, 2019, 8, 47.	7.7	35
8	Research on Scene Classification Method of High-Resolution Remote Sensing Images Based on RFPNet. Applied Sciences (Switzerland), 2019, 9, 2028.	1.3	12
9	A novel method to characterize the angular resolution of soft X-ray grazing incidence telescope. Optoelectronics Letters, 2019, 15, 98-103.	0.4	0
10	Origin of Fresnel problem of two dimensional materials. Scientific Reports, 2019, 9, 17825.	1.6	2
11	Scene classification of high-resolution remote sensing images based on IMFNet. Journal of Applied Remote Sensing, 2019, 13, 1.	0.6	8
12	Design of First-Order 121.6 nm Minus Filters. Applied Spectroscopy, 2018, 72, 1498-1502.	1.2	2
13	Design of second-order 121.6-nm narrowband minus filters using asymmetrically apodized thickness modulation. Applied Physics B: Lasers and Optics, 2018, 124, 1.	1.1	3
14	Design and Fabrication of Far-Ultraviolet Reflective Broadband Filter Based on Dielectric Materials. Applied Spectroscopy, 2018, 72, 943-946.	1.2	9
15	A new auroral boundary determination algorithm based on observations from TIMED/GUVI and DMSP/SSUSI. Journal of Geophysical Research: Space Physics, 2017, 122, 2162-2173.	0.8	25
16	Design of dual-band cold mirrors. Scientific Reports, 2017, 7, 15402.	1.6	3
17	Imaging of plasmasphere by Chang'e 3. , 2017, , .		0
18	Response of plasmaspheric configuration to substorms revealed by Chang'e 3. Scientific Reports, 2016, 6, 32362.	1.6	16

BO CHEN

#	Article	IF	CITATIONS
19	Doubleâ€peak subauroral ion drifts (DSAIDs). Geophysical Research Letters, 2016, 43, 5554-5562.	1.5	32
20	Determination of the Earth's plasmapause location from the CEâ€3 EUVC images. Journal of Geophysical Research: Space Physics, 2016, 121, 296-304.	0.8	18
21	Analysis of observational data from Extreme Ultra-Violet Camera onboard Chang'E-3 mission. Astrophysics and Space Science, 2016, 361, 1.	0.5	13
22	Hemispheric asymmetry of subauroral ion drifts: Statistical results. Journal of Geophysical Research: Space Physics, 2015, 120, 4544-4554.	0.8	15
23	EUV emissions from solar wind charge exchange in the Earth's magnetosheath: Threeâ€dimensional global hybrid simulation. Journal of Geophysical Research: Space Physics, 2015, 120, 138-156.	0.8	6
24	Design and fabrication of far ultraviolet filters based on π-multilayer technology in high-k materials. Scientific Reports, 2015, 5, 8503.	1.6	8
25	Solar cycle, seasonal, and diurnal variations of subauroral ion drifts: Statistical results. Journal of Geophysical Research: Space Physics, 2014, 119, 5076-5086.	0.8	52
26	Thermal and stress studies of the 30.4nm Mo/Si multilayer mirror for the moon-based EUV camera. Applied Surface Science, 2014, 317, 902-907.	3.1	4
27	Evolution of earth's plasmasphere in response to the solar wind variations and magnetic storms. , 2014, , .		0
28	Influence of background pressure on the microstructure and optical properties of Mo/Si multilayers fabricated by magnetron sputtering. Science China: Physics, Mechanics and Astronomy, 2013, 56, 1689-1693.	2.0	3
29	A model for thickness effect on the band gap of amorphous germanium film. Applied Physics Letters, 2013, 102, .	1.5	15
30	Moonâ€based EUV imaging of the Earth's Plasmasphere: Model simulations. Journal of Geophysical Research: Space Physics, 2013, 118, 7085-7103.	0.8	25
31	Inversion of the Earth's Plasmaspheric Density Distribution from EUV Images with Genetic Algorithm. Chinese Journal of Geophysics, 2012, 55, 1-9.	0.2	13
32	Microstructures of the interlayer in Mo/Si multilayers induced by proton irradiation. Science China: Physics, Mechanics and Astronomy, 2012, 55, 2194-2198.	2.0	1
33	Plasmaspheric trough evolution under different conditions of subauroral ion drift. Science China Technological Sciences, 2012, 55, 1287-1294.	2.0	12
34	Reconstruction of the plasmasphere from Moon-based EUV images. Journal of Geophysical Research, 2011, 116, n/a-n/a.	3.3	11
35	Deformation Twinning in Pure Nickel Induced by a High-Current Pulsed Electron Beam. Arabian Journal for Science and Engineering, 2011, 36, 663-669.	1.1	4
36	Mo/Si multilayers used for the EUV normal incidence solar telescope. Science China: Physics, Mechanics and Astronomy, 2011, 54, 406-410.	2.0	3

BO CHEN

#	Article	IF	CITATIONS
37	Roughness analysis of optical surfaces by x-ray scattering. , 2011, , .		Ο
38	Calculation of the extreme ultraviolet radiation of the earth's plasmasphere. Science China Technological Sciences, 2010, 53, 200-205.	2.0	9
39	Space solar telescope in soft X-ray and EUV band. Science in China Series G: Physics, Mechanics and Astronomy, 2009, 52, 1806-1809.	0.2	7
40	The Solar X-EUV Imaging Telescope. Chinese Journal of Geophysics, 2005, 48, 257-265.	0.2	4